

# Virus-host interactions shape viral dispersal giving rise to distinct classes of travelling waves in spatial expansions

Michael Hunter,<sup>1</sup> Tongfei Liu,<sup>1,2</sup> Wolfram Möbius,<sup>3,4</sup> and Diana Fusco<sup>1,\*</sup>

<sup>1</sup>*Cavendish Laboratory, University of Cambridge, Cambridge, CB3 0HE, United Kingdom*

<sup>2</sup>*Department of Physics, University of Oxford, Oxford, OX1 3PJ, United Kingdom*

<sup>3</sup>*Living Systems Institute, University of Exeter, Exeter, EX4 4QD, UK*

<sup>4</sup>*Physics and Astronomy, College of Engineering,*

*Mathematics and Physical Sciences, University of Exeter, Exeter, EX4 4QL, UK*

(Dated: September 25, 2020)

Reaction-diffusion waves have long been used to describe the growth and spread of populations undergoing a spatial range expansion. Such waves are generally classed as either pulled, where the dynamics are driven by the very tip of the front and stochastic fluctuations are high, or pushed, where cooperation in growth or dispersal results in a bulk-driven wave in which fluctuations are suppressed. These concepts have been well studied experimentally in populations where the cooperation leads to a density-dependent growth rate. By contrast, relatively little is known about experimental populations that exhibit a density-dependent dispersal rate.

Using bacteriophage T7 as a test organism, we present novel experimental measurements that demonstrate that the diffusion of phage T7, in a lawn of host *E. coli*, is hindered by the physical presence of the host bacteria cells. The coupling between host density, phage dispersal and cell lysis caused by viral infection results in an effective density-dependent diffusion rate akin to cooperative behaviour. Using a system of reaction-diffusion equations, we show that this effect can result in a transition from a pulled to pushed expansion. Moreover, we find that a second independent density-dependent effect on phage dispersal spontaneously emerges as a result of the viral incubation period, during which phage is trapped inside the host unable to disperse. Our results indicate both that bacteriophage can be used as a controllable laboratory population to investigate the impact of density-dependent dispersal on evolution, and that the genetic diversity and adaptability of expanding viral populations could be much greater than is currently assumed.

## I. INTRODUCTION

Spatial range expansions are ubiquitous in nature, from the expansion of invasive plant species, through the migration of ancient human populations, to the range shifts of many organisms to higher altitudes and latitudes due to climate change [1–8]. One of the hallmarks of spatial expansions is the rapid loss of genetic diversity due to the enhanced fluctuations at the front [9, 10]. This effect can, however, be significantly mitigated in the presence of density-dependent growth [11, 12], such as an Allee effect [13], or density-dependant dispersal, where individuals in highly dense patches tend to disperse more quickly [14]. In particular, it has recently been shown theoretically that the ratio between the deterministic velocity of the front and that of its linearized approximation is sufficient to classify the expansions in three distinct types of travelling waves, nominally pulled, semi-pushed and fully-pushed, which respectively exhibit qualitatively distinct behaviors in the decay of heterozygosity, the stochastic wandering of the front position, and the probability distribution of the most recent common ancestor [14, 15].

Because density-dependent growth can play such a crucial role in the evolutionary dynamic of a population, it

has been extensively investigated in both naturally occurring range expansions in animals, such as the invasions of both Eurasian gypsy moths and house finches in North America [16, 17], and in laboratory microbial model systems, where the expansion dynamics in populations of the budding yeast *Saccharomyces cerevisiae* transition from pulled to pushed as growth becomes more cooperative [18], with a corresponding preservation of genetic diversity [19]. In comparison, relatively little is known about the population dynamic of experimental systems that exhibit density-dependant dispersal, even if it has been documented in several natural populations [20] and the transition to pushed waves has been theoretically predicted [14].

One laboratory system that has been hypothesized to undergo density-dependent dispersal is bacteriophage expanding in a bacterial lawn. The crowded bacterial environment is thought to hinder phage diffusion because of steric interactions, resulting in a density-dependent diffusion rate due to the coupling between the host and the viral population densities [21]. Direct experimental quantification of this density-dependent diffusion is, however, very limited [22], and its consequence on the front population dynamic mostly unknown.

Here, we address the open questions of (i) whether and how the rate of phage diffusion depends on the density of surrounding bacteria, (ii) under what conditions transitions to semi-pushed and fully-pushed expansions can occur, and (iii) what role density-dependent diffusion

---

\* E-mail: df390@cam.ac.uk

plays in this. We first design an experimental protocol to measure the dependence of the phage diffusion rate on the density of surrounding bacteria. We then construct a system of reaction-diffusion equations to determine the phage front velocity, demonstrating that transitions to both semi-pushed and fully-pushed waves can occur. We find that the presence and location of these transitions are controlled by two independent effects that alter the density-dependent diffusion of the virus: the first is associated with the steric interactions with the surrounding bacteria, while the second spontaneously emerges from the viral infection dynamic, which prevents a viral particle from diffusing during infection of the host.

Taken together, our results identify bacteriophages as a controllable laboratory model system to investigate the role of density-dependent dispersal in evolution and provide a quantitative explanation of the physical processes that control the phage population dynamic during a range expansion. Going beyond phages, our findings suggest that a broad range of viruses may expand via pushed travelling waves and, consequently, may be much more adaptable than previously thought.

## II. EXPERIMENTAL MEASUREMENTS OF DENSITY-DEPENDENT DISPERSAL IN COLIPHAGE T7

Starting with Yin and McCaskill [21], it is usually recognized that bacteria can act as a barrier to phage diffusion, resulting in a diffusion rate that depends on the bacterial density. This dependence is indeed necessary in phage expansion models to correctly reproduce the non-monotonicity of front velocity observed as a function of bacterial density [21, 23–25]. Despite its importance, the dependence of phage diffusion rate on bacterial density has never been measured experimentally, possibly because direct observation of phage diffusion in a dense bacterial environment using optical microscopy is exceedingly challenging.

To address this problem, we designed an experimental setup that leverages the different interactions between phage and two bacterial strains, one resistant and one susceptible to the virus. Phage droplets were inoculated on a uniform background of resistant *E. coli* of tunable density placed on top of an agar plate. Since phage adsorption is assumed to be prevented in this strain [26, 27], the resistant bacteria serve as passive barrier to phage dispersal. To probe the phage location, several droplets of susceptible *E. coli* were placed at different distances from the phage droplets. The time  $\Delta t$  required by the phage to travel the distance  $r$  between a viral droplet and a close-by susceptible bacteria droplet was monitored *in vivo* by tracking the appearance of clearings in the susceptible droplets (Fig. 1a and b).

By gathering statistics over many droplet-droplet pairs, we were able to first confirm that the relationship between distance travelled and mean first passage time is

consistent with diffusive behavior for the whole range of background densities tested (Fig. 1b), and then calculate the rate of phage diffusion  $D$  as a function of background bacterial density (Fig. 1c).

Building on previous efforts to account for density-dependence in plaque models [21], we fit our data using Fricke’s Law [24, 28], which describes the diffusion of a solute through a suspension of spheroids [29]:

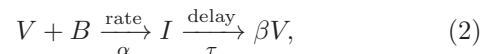
$$D = \frac{1-b}{1+\frac{b}{\eta}} D_0 \quad ; \quad b = \frac{B}{B_{max}}, \quad (1)$$

where  $b$  indicates the fraction of bacteria  $B$  relative to a maximum value  $B_{max}$  and  $\eta$  accounts for the shape of the cells: spherical cells correspond to  $\eta=2$ , while *E. coli* cells have previously been determined to correspond to  $\eta=1.67$  [24]. Our experimental data allow for the first time to estimate the two fitting parameters required by Fricke’s law in this context: the free diffusion rate  $D_0$  (i.e. the diffusion rate in the absence of surrounding bacteria), and the bacterial density  $B_{max}$  at which diffusion is expected to be completely halted. We estimate  $D_0 = 4.13 \pm 0.19 \mu\text{m}^2/\text{s}$ , which is in good agreement with the rate of  $4 \mu\text{m}^2/\text{s}$  previously determined by Ouchterlony double immunodiffusion in 10 g/l agar of phage P22 (similar size and shape of T7) [30, 31]; and  $B_{max} = 2.16 \pm 0.19 \mu\text{m}^{-2}$ , which is consistent with the typical dimensions of an *E. coli* cell (assuming *E. coli* cells are approximately  $0.5 \times 2 \mu\text{m}$ , we would expect a  $1 \mu\text{m}^2$  cross section to contain between 1 and 4 closely packed cells, depending on their orientation and deformation).

## III. MODELLING PLAQUE GROWTH: DENSITY-DEPENDENT DIFFUSION AND ADSORPTION TO INFECTED CELLS

To investigate whether the phage expansion on a bacterial lawn occurs as a pulled or a pushed wave, and to uncover the role of host density-dependence, we compare the actual front velocity with the velocity  $v_F$  of the corresponding linearized system, as their ratio has been shown to be sufficient to determine the wave class in single species range expansions [15]. To this end, we develop a mathematical model that accommodates the density-dependent diffusion we have experimentally measured.

We model the spatial dynamics of bacteriophage plaque growth by considering the interactions between three populations: viruses (phage)  $V$ , uninfected host bacteria  $B$  and infected host bacteria  $I$ , similar to [21, 23–25, 32–35]. The process may be summarised as



where  $\beta$  is the burst size,  $\alpha$  is the rate of adsorption, and  $\tau$  is the lysis time.

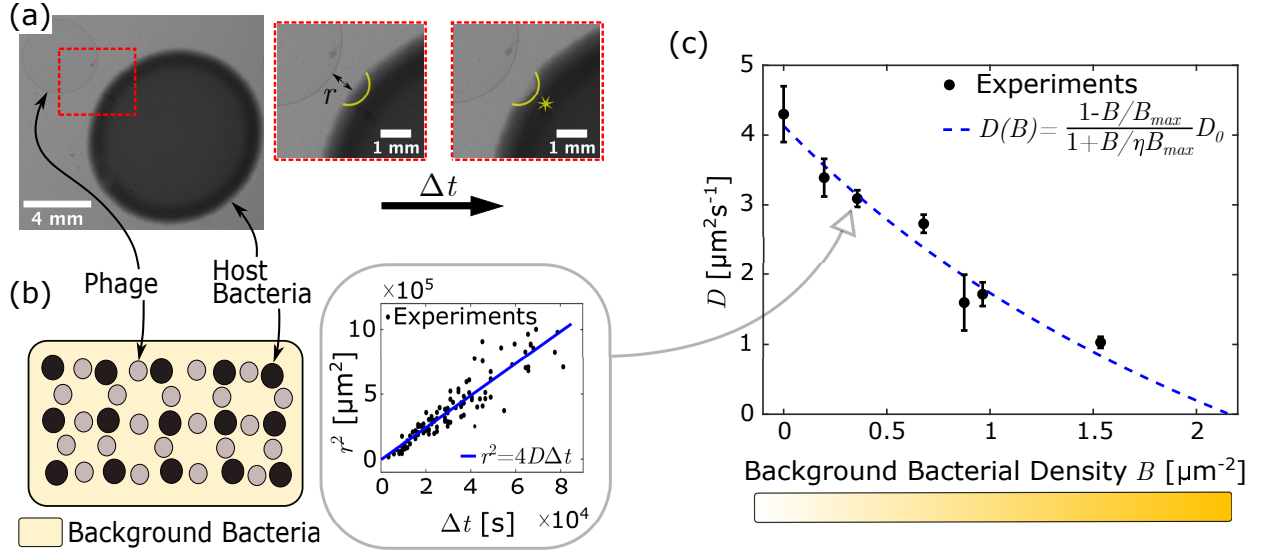


FIG. 1. Experiments show how rate of phage diffusion is reduced by surrounding bacteria. (a): The basis of the experimental set-up, consisting of a droplet of phage and host bacteria, separated by a distance  $r$ . After time  $\Delta t$ , a plaque begins to form in the host bacterial droplet (starred region). (b): The full experimental set-up, consisting of many phage-host droplet pairs on top of a lawn of phage resistant bacteria of variable density. The presence of chloramphenicol in the plate media ensures that the background bacterial density is constant over the course of the experiment (see Methods). An example plot of  $r^2$  against  $\Delta t$  data, with linear fit, for a resistant bacteria density of  $0.36 \mu\text{m}^{-2}$  is shown. (c): The diffusion rate obtained as a function of resistant bacteria density (i.e. for several instances shown in (b)), fit with Fricke's Law (Eq. 1).

As the model is deterministic, without loss of generality, we describe these populations with a set of reaction-diffusion equations in 1D, similar to those examined by Jones *et al.* [32]:

$$\frac{\partial B}{\partial t} = -\alpha V B, \quad (3a)$$

$$\frac{\partial I}{\partial t} = \alpha V B - \alpha V_{t-\tau} B_{t-\tau}, \quad (3b)$$

$$\frac{\partial V}{\partial t} = \frac{\partial}{\partial x} \left( D \frac{\partial V}{\partial x} \right) - \alpha V B - \alpha^* V I + \beta \alpha V_{t-\tau} B_{t-\tau}, \quad (3c)$$

where  $V$ ,  $B$  and  $I$  indicate the concentration of the population as a function of space and time. The subscript is used to indicate that those terms are evaluated at time  $t - \tau$ .  $D$  is the density-dependent diffusion coefficient of the phage, which we experimentally fit to Fricke's law in the previous section (Eq. 1).  $\alpha^* = \alpha$  or  $\alpha^* = 0$ , depending on whether adsorption to previously infected hosts is allowed or prevented, respectively. We assume that the host bacteria are motionless and neglect desorption.

Our model introduces two ingredients that are biologically and physically relevant, and that are expected to affect the front dynamic. First, in contrast to previous work [21, 23–25, 33–35], where the diffusion coefficient  $D$  only depends on the initial bacterial concentration  $B_0$  ( $b = \frac{B_0}{B_{max}}$  in Eq. 1), we allow  $D$  to vary in time and space according to the local bacterial density ( $b = \frac{B+I}{B_{max}}$

in Eq. 1), resulting in faster diffusion inside the phage clearing (Fig. 2a). Secondly, we allow for the possibility that phage can adsorb to previously infected cells ( $-\alpha^* V I$  term in Eq. 3c), as is the case for phage T7. The presence or absence of these two effects generates four model variants that are summarized in Fig. 2a: Uniform vs. Variable Diffusion model (UDM vs. VDM), and adsorption vs. non-adsorption to infected cells (+ vs. -).

In line with previous studies, we cast the equations using dimensionless variables. We measure concentrations in terms of the initial bacterial density  $B_0$ , time in units of  $\tau$ , and length in units of  $L = \sqrt{D(B_0)\tau}$  (the distance diffused within a lysis time at the front). This results in the following set of dimensionless variables:  $\bar{B} \equiv B/B_0$ ,  $\bar{I} \equiv I/B_0$ ,  $\bar{V} \equiv V/(\beta - 1)B_0$ ,  $\bar{t} \equiv t/\tau$ ,  $\bar{x} \equiv x/L$  and  $K \equiv \alpha\tau B_0$ . Consequently,  $\bar{c} = c\sqrt{\tau/D}$ , where  $\bar{c}$  and  $c$  are the dimensionless and dimensional velocity of the expansion front, respectively (Fig. 2a).

In these units, the UDMs are characterized by a constant dimensionless diffusion coefficient  $\bar{D} = D\tau/L^2 = 1$  by definition, while the VDMs exhibit a dimensionless density-dependent diffusion coefficient of the form:

$$\bar{D} = \frac{1 - f(\bar{B} + \bar{I})}{1 + f(\bar{B} + \bar{I})/\eta} \cdot \frac{1 + f/\eta}{1 - f}, \quad (4)$$

where  $f = B_0/B_{max}$  is the initial fraction of bacteria. It is important to note that  $\bar{D}$  from Eq. 4 is always greater than or equal to 1, and can therefore be interpreted as a “boost” in diffusion that the VDMs exhibit in the bulk of the plaque in comparison to the correspond-

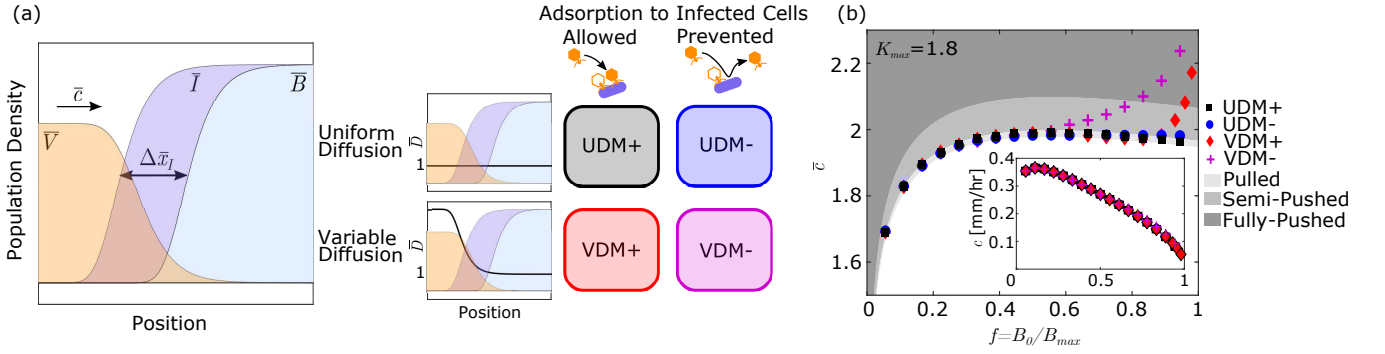


FIG. 2. (a): A sketch of the population concentrations  $\bar{B}$ ,  $\bar{I}$  and  $\bar{V}$  as a function of location at the expansion front (the precise location is not important here, as the qualitative shape of the fronts remain constant during the expansion). The front is propagating with dimensionless velocity  $\bar{c}$  to the right. The dimensionless width  $\Delta\bar{x}_I$ , characterising the width of the infected region is given by the difference in position of the uninfected ( $\bar{B}$ ) and infected fronts ( $\bar{B} + \bar{I}$ ). The differing diffusion and adsorption behaviours explored lead to four different model variants in this work. Variants either have a Uniform or Variable diffusion rate (UDM or VDM respectively), and adsorption to previously infected cells either does (+), or does not (-) occur, leading to the four model variants (UDM+, UDM-, VDM+ and VDM-). (b): Dimensionless front velocity  $\bar{c}$  as a function of bacteria fraction  $f$ , with shaded regions indicating the different expansion types. Error bars on the velocities are smaller than the symbols. Inset also shows the dimensional velocity  $c$ . Model parameters are chosen to represent typical T7 expansions with  $\beta = 50$ ,  $\tau = 18$  mins, and  $\alpha B_{max} = 0.1 \text{ min}^{-1}$  [21, 32, 35], corresponding to  $K_{max} = 1.8$  in our model.

ing UDMs. This boost mathematically describes the decrease in steric interactions between phage and bacteria due to the lysis of the host as the viral infection proceeds (black line in Fig. 2a).

In terms of these variables, our model (Eqs. 3) becomes:

$$\frac{\partial \bar{B}}{\partial \bar{t}} = -K(\beta - 1)\bar{V}\bar{B}, \quad (5a)$$

$$\frac{\partial \bar{I}}{\partial \bar{t}} = K(\beta - 1)\bar{V}\bar{B} - K(\beta - 1)\bar{V}_{\bar{t}-1}\bar{B}_{\bar{t}-1}, \quad (5b)$$

$$\frac{\partial \bar{V}}{\partial \bar{t}} = \frac{\partial}{\partial \bar{x}} \left( \bar{D} \frac{\partial \bar{V}}{\partial \bar{x}} \right) - K\bar{V}\bar{B} - K^*\bar{V}\bar{I} + \beta K\bar{V}_{\bar{t}-1}\bar{B}_{\bar{t}-1}, \quad (5c)$$

where  $K = \alpha\tau B_0$  and  $K^* = \alpha^*\tau B_0$ .

From Eqs. 5 three natural parameters emerge: the dimensionless adsorption coefficient  $K = \alpha\tau B_0$ , the burst size  $\beta$  and the dimensionless diffusion coefficient  $\bar{D}$ . In the UDMs,  $\bar{D} = 1$ , leaving  $K$  and  $\beta$  as the only two parameters of the model. By contrast, in the VDMs,  $\bar{D}$  is a function of  $B_0$  (Eq. 4), which entangles the effect of initial bacterial density on  $K$  and  $\bar{D}$ . To decouple adsorption and diffusion, we define a set of three new independent parameters that we will use in the following to analyse the model variants: the initial fraction of bacteria  $f = B_0/B_{max}$ , the maximum dimensionless adsorption coefficient  $K_{max} = \alpha\tau B_{max}$  ( $K = fK_{max}$ ), and the burst size  $\beta$ .

#### IV. FROM PULLED, TO SEMI-PUSHED TO FULLY PUSHED

By numerically solving the PDE system in Eqs. 5, we obtain the front velocity  $\bar{c}$  and compare it with the velocity  $\bar{c}_F$  of the linearised approximation of the model (see Methods for details). Because the linearised approximation describes the population dynamic at the very tip of the phage front, where  $\bar{I} \approx 0$  and  $\bar{D} \approx 1$ ,  $\bar{c}_F$  is the same for all four model variants and, therefore, depends only on the dimensionless adsorption coefficient  $K = fK_{max}$  and the burst size  $\beta$  - see Methods. In addition to front velocity, we also determine the characteristic width of the infection region  $\Delta\bar{x}_I$  (Fig. 2a), which we will discuss later on.

The transitions between different travelling wave regimes are then determined from the ratio  $\frac{\bar{c}}{\bar{c}_F}$  according to Ref. [15]: (i) pulled waves for  $\frac{\bar{c}}{\bar{c}_F} = 1$ , (ii) semi-pushed wave for  $1 < \frac{\bar{c}}{\bar{c}_F} < \frac{3}{2\sqrt{2}}$ , (iii) fully pushed waves for  $\frac{\bar{c}}{\bar{c}_F} \geq \frac{3}{2\sqrt{2}}$  (see Methods). An example of these transitions in the different model variants for a set of infection parameters typical of T7 is shown in Fig. 2b. Under these conditions, we observe that the UDM+ exhibits a pulled wave for the full range of initial bacterial fraction, while the UDM-, the VDM+ and the VDM- waves become increasingly more pushed as  $f$  increases. In terms of dimensional velocity, the difference between the model variants is minimal (inset in Fig. 2b), justifying why these effects have gone unnoticed in past theoretical work that aimed at predicting experimental phage front speeds.

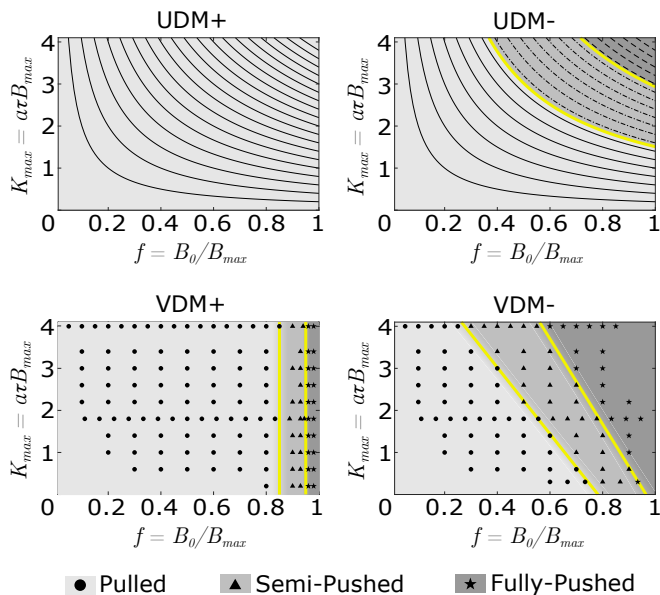


FIG. 3. Phase diagrams showing the expansion types for the four model variants as a function of bacterial density  $f$  and maximum dimensionless adsorption coefficient  $K_{max}$  - burst size  $\beta=50$  throughout. Lines in the UDMs, and data points in the VDMs indicate the parameter combinations for which numerical integration was performed, and velocities calculated. These values are interpolated to estimate the transition boundaries between different classes of travelling waves (yellow lines). In the UDM+, we do not observe pushed transitions, while in the VDM+ transitions occur at approximately constant bacteria fractions. In the UDM-, as  $K$  and  $\beta$  are the only free parameters, transitions occur at specific values of  $K$ . In the VDM-, the transitions are heuristically approximated as linear relationships between  $K_{max}$  and  $f$ .

### A. Wave Transitions are Very Sensitive to Virus-Host Interactions

To generalise our findings and fully characterise the origin and nature of the transitions in front dynamic for the different model variants, we extend our investigation to a broader range of parameter values, by varying  $K_{max}$  (and  $\beta$ , see Appendix B) about the typical parameters used in Fig. 2b.

Fig. 3 shows the type of expansion that occurs in each of the models as a function of  $f$  and  $K_{max}$ . The results clearly indicate that the presence or absence of density-dependent diffusion and adsorption to infected cells can dramatically alter the type of travelling wave undergone by phage, with the UDM+ being the only model resulting in a pulled population wave for the whole range of parameters explored. In the following, we will provide a physical interpretation for these observations, by identifying two independent effects that alter phage dispersal in a density-dependent fashion.

### B. Decreased Steric Effects due to Host Lysis Promote the Transition to Pushed Waves at High Bacterial Densities

The first effect can be appreciated by comparing the phase diagram of the UDM+ to that of the VDM+, and is a direct consequence of the variable diffusion coefficient that our model *explicitly* introduces in Eq. 4.

In the VDM+, transitions to semi-pushed and fully pushed waves occur at high values of  $f$  with very weak dependence on  $K_{max}$ . This results from the boost in phage diffusion that occurs in the bulk of the plaque as host cells lyse and steric effects decrease. Because the boost increases with increasing difference in bacterial density between the front ( $\bar{B} = B/B_0 = 1$ ) and the back ( $\bar{B} = 0$ ), higher initial bacterial density  $f$  will generate a stronger boost. Beyond a given threshold, controlled exclusively by  $f$ , the phage behind the propagating front will disperse sufficiently fast to be able to catch up with the front and generate a semi-pushed or even a fully-pushed wave. For what follows, it is useful to name this explicit boost to diffusion  $\bar{D}_{exp}$ , which is mathematically identical to the dimensionless diffusion coefficient in Eq. 4, and reaches its maximum in the bulk of the plaque where no bacteria are left (Fig. 2a and dashed red line in Fig. 4b).

### C. A second “Implicit” Density-Dependent Diffusion Emerges from the Viral Infection Dynamics

Since the UDMs lack the explicit density-dependent diffusion, the appearance of transitions to pushed regimes in the UDM- may seem surprising (Fig. 3). To understand the origin of these transitions, it is helpful to consider the effects of the parameter  $K = \alpha\tau B_0$  that controls the transition. Adsorption and incubation (quantified by the parameter  $K$ ) are not only key for the effective growth rate of the phage population, but also for the effective dispersal rate of the phage, as they control the time and the probability that phage particles are “trapped” in a host cell, unable to disperse. As  $K$  increases, either *more* phage adsorb to host cells at the front per unit of time, or they are trapped there for *longer*, resulting in a hampered dispersal of the phage at the front (Fig. 4a).

To quantify this reduced dispersal, we consider a system of point-like phage particles diffusing across a field of completely permeable “sticky” obstacles, mimicking host bacteria that trap phage for a time  $\tau$ . A simple analytical argument (see Methods), supported by two-dimensional Monte Carlo simulations (Appendix A), demonstrates that the particles in this system exhibit a hindered diffusion  $D$  compared to their free diffusion  $D_0$ , such that

$$\frac{D}{D_0} = D_{imp} = \frac{1}{1 + bK_{max}}, \quad (6)$$

where  $b$  is the local bacterial density (similarly to Eq. 1).

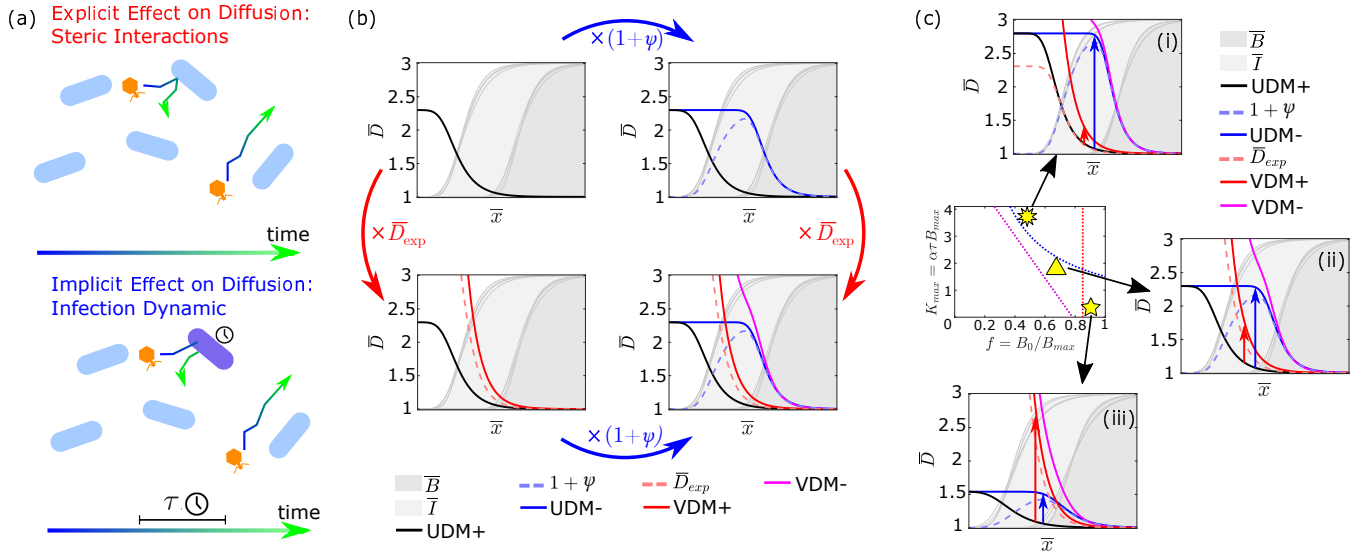


FIG. 4. (a): An illustration of both explicit and implicit effects to phage diffusion. Due to the explicit effect, phage diffusion is hindered by steric interactions with bacterial hosts, while the implicit effect hinders phage diffusion by trapping the virus for a period  $\tau$  during which it cannot disperse. (b): Proxies for the diffusive behaviour in each of the model variants plotted as a function of position across the expansion front. The base diffusion rate  $\bar{D}_{imp+}$  (Eq. 7) in the UDM+ (black solid line) is modified either by the term  $1 + \psi$  (blue arrow and blue dashed line) in the UDM- (blue solid line), which accounts for the now unhindered diffusion in the region of infected cells, or by an additional term  $\bar{D}_{exp}$  (red arrow and red dashed line) in the VDM+ (red solid line) which accounts for the hindrance due to steric effects. Both modifications occur in the VDM- (magenta line). Faint grey lines indicate the different front profiles from the model variants used to calculate the diffusion rate profiles (see Methods). (c): Diffusion profiles for three representative cases are shown, all highlighted in comparison to the semi-pushed transition boundaries for the models shown in Fig. 3: (i) high  $K_{max}$  and low  $f$ , where the UDM- and VDM- are pushed; (ii) intermediate  $f$  and  $K_{max}$ , where only the VDM- is pushed; (iii) low  $K_{max}$  and high  $f$ , where the VDM+ and VDM- are pushed. Red and blue arrows highlight the shift from the UDM+ to the VDM+ and UDM- respectively at the position where the viral profile is approximately 3/4 times its steady-state.

Because of the dependence on the local bacterial density, the phage behind the front will diffuse faster relative to the phage at the front, and might be able to catch up and contribute to the advancement of the expansion.

When adsorption to infected cells occurs (UDM+), infected cells *trap* phage as much as uninfected cells ( $b = (B + I)/B_{max}$  in Eq. 6) resulting in a dimensionless diffusion coefficient of the form

$$\bar{D}_{imp+} = \frac{1 + K}{1 + (\bar{B} + \bar{I})K}. \quad (7)$$

By contrast, when adsorption to infected cells is prevented (UDM-), phage can no longer become trapped in the infected region behind the front ( $b = B/B_{max}$  in Eq. 6), so that

$$\bar{D}_{imp-} = \frac{1 + K}{1 + \bar{B}K}. \quad (8)$$

Comparison between the two expressions (black vs. blue lines in Fig. 4b, Methods) shows that preventing adsorption to infected cells is equivalent to a boost in implicit diffusion in the infected region just behind the front, which can be approximated to

$$\frac{\bar{D}_{imp-}}{\bar{D}_{imp+}} = 1 + \psi \approx 1 + \frac{\bar{I}K}{1 + \bar{B}K}, \quad (9)$$

(blue dashed line in Fig. 4b). This boost is sufficient to shift the fast diffusing phage closer to the expanding front and, if  $K$  is sufficiently large, to generate a transition to pushed waves.

It is important to point out that this implicit density-dependent diffusion emerges spontaneously from the viral infection dynamics (common to most viruses), where infecting viruses trapped in the host cannot contribute to the advancement of the front until they are released from the host. As a consequence, unlike the explicit density-dependent diffusion, this effect cannot be easily accommodated into the diffusion coefficient of our model, as it does not act independently of the infection and growth processes. Reciprocally, it also cannot be turned-off, but is always acting in any spatial viral model exhibiting a non-zero incubation time. Nonetheless, our analysis reveals that its effects on the viral expansion dynamic becomes significant in the range of infection parameters explored here, only if adsorption to infected cells is prevented (from + to - models), or, equivalently, when the infected region implicit boost  $1 + \psi$  is present.

### D. Implicit and Explicit Density-Dependent Diffusions Act Independently with Multiplicative Effects

Because the implicit and explicit boosts to diffusion discussed above have different physical origins and are controlled by different parameters ( $K$  and  $f$ , respectively), they play significant roles in different regions of parameter space. The implicit boost that results from a lack of adsorption to infected cells, encoded in  $(1 + \psi)$ , is stronger at large  $K_{max}$ , where more phages are trapped by hosts for a longer period of time. Instead, the explicit boost caused by steric interactions, encoded in  $\bar{D}_{exp}$ , is dominant at low  $K_{max}$ . The ratio of the two effects over parameter space is shown in Appendix C, Fig. 11.

Extending the analytical argument with which we defined the implicit boost to diffusion, we can show that, to a first approximation, explicit and implicit effects act independently over a basal diffusion coefficient (see Methods). As a consequence, preventing adsorption to infected cells corresponds to multiplying the diffusion coefficient by  $1 + \psi$  (from + to - models, blue arrows in Fig. 4). Similarly, including steric effects corresponds to multiplying the diffusion coefficient by  $\bar{D}_{exp}$  (from UD to VD models, red arrows in Fig. 4). As a result, we can write the dimensionless diffusion coefficient of the VDM-, which exhibit both effects, as

$$\bar{D}_{VDM-} = (1 + \psi)\bar{D}_{exp}\bar{D}_{imp+}, \quad (10)$$

where all the terms are calculated with respect to  $\bar{B}$  and  $\bar{T}$  from the VDM- simulations.

In contrast to the other models, this function depends non-trivially on  $K_{max}$  and  $f$ , making it challenging to find a simple parameter combination that controls the transitions to pushed waves. Nonetheless, we see that the diffusion coefficient determined at  $3/4$  times the steady state phage population is able to qualitatively capture the behavior of the transition lines in all models (Fig. 5) and it explains why the VDM- approaches the UDM- and the VDM+ at high and low  $K_{max}$ , respectively, where either effects dominate (Fig. 3 and Fig. 4c). While the phage diffusion at a specific population density is not sufficient to recapitulate pushed behavior, which by definition depends on the whole wave dynamic, Fig. 5 illustrates that regions in parameter space with similar effective diffusion within a model correspond to similar types of expansions. This supports the idea that the density-dependent diffusion, whether implicit or explicit, is the key ingredient that leads to transitions to pushed waves.

### E. Reduced Burst Size Results in a More Pushed Expansion

Fig. 3 illustrates the transition to pushed expansions for a fixed burst size  $\beta$ . Because burst size affects the growth rate of the phage and, consequently, its expansion velocity, it is natural to wonder whether it also has

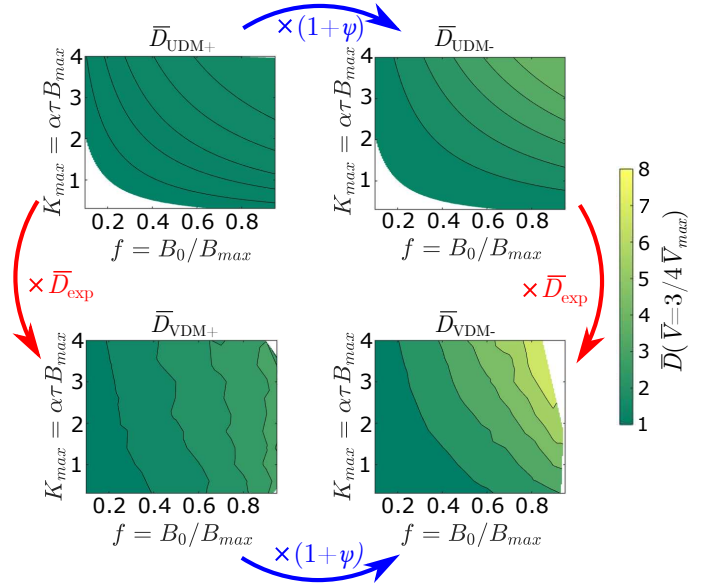


FIG. 5. Dimensionless diffusion rates in each of the models determined at the front position where the phage population is  $3/4$  times the steady state population  $\bar{V}_{max}$ , plotted as a function of both  $f$  and  $K_{max}$ . Contour lines indicate levels of constant  $\bar{D}$ . The behaviour of the contours qualitatively matches that of the transition boundaries in Fig. 3.

any effect on the transitions between expansion types. Interestingly, we find that the general shape of the transitions for the model variants does not change when decreasing  $\beta$  by a factor of 2 (Fig. 8), in line with the idea that density-dependent dispersal is the main driver to alterations in wave dynamics. The exact location of the transitions, however, are slightly affected by the burst size (Fig. 9). The similarity between the transition positions as a function of burst size and the corresponding velocity  $\bar{c}_F$  (Fig. 10) suggest that decreasing burst size slows down the very front of the wave facilitating the transition to pushed regimes. A more detailed discussion of the influence of burst size can be found in Appendix B.

## V. DISCUSSION

In this work, we have demonstrated experimentally that the diffusion of phage in a bacterial lawn is hindered by steric interactions with the host bacterial cells, resulting in a density-dependent diffusion coefficient which we have quantified. Going beyond current descriptions of plaque growth, which have considered host density-dependence only for setting a constant diffusion rate parameter, we construct a reaction-diffusion model of the phage-bacteria system that explicitly incorporates a diffusion rate that depends on local host density, and therefore varies in time and space. We show that this effect can lead to the transition to pushed waves at high host densities. We also show that a second, independent density-dependence in diffusion emerges implicitly from

the underlying viral dynamics, whereby phage are unable to diffuse during replication within the host. We find that when adsorption to infected host cells is prevented, this effect can also lead to the transition to pushed waves. Together, this indicates that bacteriophage offer an excellent experimental system to study the effect of density-dependent diffusion on expansion dynamic.

### A. Eco-Evolutionary Consequences of Density-Dependent Dispersal

The transition from a pulled wave to a pushed wave has traditionally been associated with increased cooperativity between individuals, quantified by density-dependent growth, or more recently, density-dependent dispersal [13–15]. By analogy, the density-dependence in phage diffusion can be interpreted as an emergent cooperativity, which stems from the fact that as phage work together towards cell lysis, they remove bacterial obstacles, indirectly favouring the dispersal of neighboring phage. The fact that the diffusion is dynamically changed as phage replicate could lead to interesting ecological feedback. Ecological feedback on diffusion has been shown in other contexts to theoretically lead to pattern formation, and in some cases help maintain genetic diversity and mitigate the risk of extinctions [36]. Indeed, density-dependent dispersal has been shown to be a key ingredient in a generic route to pattern formation in bacterial populations [37].

It has also been shown that pushed dynamics in range expansions have significant consequences for the evolution of the population. In pulled expansions, the high susceptibility to stochastic fluctuations results in inefficient selection which can lead to the accumulation of deleterious mutations, known as expansion load [38, 39]. This has been demonstrated previously in experimental microbial populations [40–42]. By contrast, in fully pushed waves, the genetic drift is reduced [12], potentially leading to more efficient selection and a reduced risk of accumulating deleterious mutations. Even in the case of semi-pushed waves, where fluctuations are high, the growth and ancestry processes are localised behind the tip of the front, thereby suppressing the strong founder effect found in pulled expansions [14, 15]. Our results suggest that expanding populations of viruses might be subject to more efficient selection compared to other species, e.g. microbes, and be better equipped to adapt to new environments.

### B. Relevance to Real Viral Species

We find that the transition to a pushed wave can occur due to two separate effects: an explicit density-dependent diffusion rate, caused by steric interactions between the phage and the host bacteria, which is dominant in crowded host environments, and an implicit hin-

drance to the diffusion of the phage population at the front caused by the viral infection dynamics. The evolutionary benefit of reducing genetic drift is expected to be strongest in populations that experience both effects and where adsorption to infected host is limited (VDM-). Some bacteriophage have mechanisms that prevent adsorption to already infected cells, usually by blocking receptor sites post-infection [43]. Bacteriophage T5 produces a lipoprotein (Lip) that is expressed at the beginning of infection, preventing superinfection by blocking its own receptor site (FhuA protein), and protecting newly produced phage from inactivation by binding to free receptors released by lysed cells [44, 45]. Similar mechanisms are also well documented in several temperate phage. Phage  $\Phi$ V10 possesses an O-acetyltransferase that modifies the specific  $\Phi$ V10 receptor site (the O-antigen of *E. coli* O157:H7) to block adsorption [46]. Similarly, *Pseudomonas aeruginosa* prophage D3 modifies the O-antigen of LPS on the host surface to prevent adsorption of the many phage that bind to the O-antigen [47]. This is similar to other *Pseudomonas* prophage which encode for twitching-inhibitory protein (TiP) that modifies the type IV pilus on the *P. aeruginosa*, preventing further adsorption [48, 49].

Indeed, mechanisms to prevent superinfection by preventing adsorption to infected cells have been observed in viruses beyond bacteriophage [50]. For instance, cells recently infected with Vaccinia virus VacV (the live vaccine used to eradicate smallpox) express two proteins that repel super-infecting virions, resulting in plaques that grow four-fold faster than would be expected by replication kinetics alone [51]. Our results show that even in absence of explicit steric effects, pushed expansions can occur if adsorption to infected hosts is prevented (UDM-), as is the case for VacV, suggesting that pushed waves might be more widespread than previously thought among different viral systems.

As much as it may be evolutionarily advantageous for the viral population to undergo a pushed expansion, it would be just as advantageous for the host cells to prevent this from happening. From the host’s point of view, it would likely be beneficial if infected cells were able to adsorb as many virions as possible. According to our model (VDM+), this would reduce the effect of the implicit density-dependent hindrance to diffusion, leaving only the explicit effect to act at very high host concentrations.

### C. Life History Parameters in Spatial Settings

Our experiments have shown that the rate of phage diffusion strongly depends on the host environment and, in particular, can dramatically differ from liquid culture measurements, where even at high overnight densities of  $\sim 10^9$  cells/ml, the volume fraction occupied by the cells is  $\sim 0.001$ , and so diffusion is effectively unhindered. This realisation raises the question of whether other phage life



history parameters depend strongly on the surrounding host environment. Traditionally, these parameters are determined by experiments carried out in a well mixed liquid culture [24, 52]. It is perfectly possible that these parameters could take significantly different values when the infection occurs in different spatially structured environments and varying metabolic states of the host cells [53]. Moreover, it is possible that these parameters are not only different on solid media when compared to liquid, but may also vary across the expansion in a similar fashion to the diffusion rate. For instance, upon lysis, release of cytoplasmic fluids could affect the infection or lysis of neighbouring cells, resulting in life-history parameters that vary with cell density.

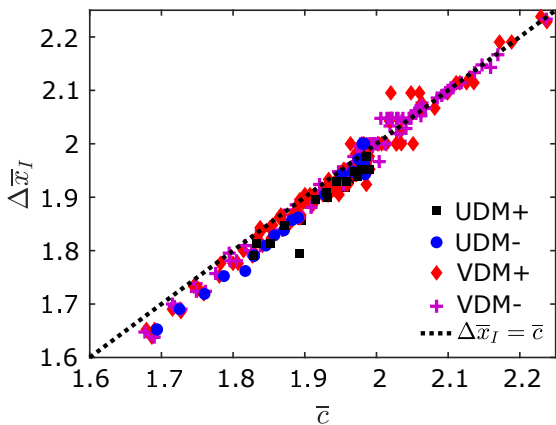


FIG. 6. Dimensionless width  $\Delta\bar{x}_I$  shown to be equal to  $\bar{c}$  for all models across the range of  $f$  and  $K_{max}$  investigated in Fig. 3, corresponding to an expansion that travels the width of the infected region every lysis time. We attribute the small discrepancy observed at lower values to the limited convergence of the front profile to its steady-state because of trade-offs between precision and computational cost.

In this context, our findings suggest a way to measure lysis time on solid media and over time during a plaque expansion. Lysis time is traditionally measured on liquid media, since it requires periodic and precise sampling of the phage population, which is challenging to perform on agar plates. The models presented in this paper, which assume a deterministic lysis time, produce a front which expands by the width of the infected region  $\Delta\bar{x}_I$  during one lysis time interval. As a result, the dimensionless infection region width  $\Delta\bar{x}_I$  is equivalent to the dimensionless velocity  $\bar{c}$ , as predicted in all the models and confirmed by the numerics (Fig. 6). By utilising phage engineered to result in fluorescent infected cells [54], imaging a growing plaque of such phage over time in both fluorescent and bright-field channels should yield information about the distributions of infected and uninfected bacteria (see Fig. 2a), and allow one to determine the dimensional equivalent of  $\Delta\bar{x}_I$ . By simultaneously measuring the velocity of the expansion, the lysis time in solid media and its variation during the course of an

expansion could be estimated.

#### D. Inferring the Fisher Velocity in Experimental Systems

While this work provides theoretical predictions and physical insights regarding the transition from pulled to pushed waves in phage expansions, it also shows that phage plaques represent a well-controlled model system to investigate these different population dynamics experimentally. To test our results experimentally, however, we need to determine the velocity ratio  $c/c_F$ . In contrast to simulations, the velocity of the linearized system  $c_F$  cannot be directly measured in experiments, but it could be inferred by measuring the parameters that contribute to it. One possible route could consist in collapsing the growth and spread of the phage into a single reaction-diffusion equation, namely:

$$\frac{\partial n}{\partial t} = \frac{\partial}{\partial x} \left( D(n) \frac{\partial n}{\partial x} \right) + nr(n), \quad (11)$$

where  $n$  represents the density of phage, while  $r(n)$  and  $D(n)$  are respectively the density dependent growth and diffusion rate of phage, that would implicitly describe the processes of diffusion, adsorption, replication and lysis. The Fisher velocity of this model is  $c_F = 2\sqrt{r(0)D(0)}$ , where  $r(0)$  and  $D(0)$  are the growth and diffusion rate at low density, respectively [55]. In principle, both of these quantities could be measured experimentally, without the need to determine the full dependence of  $r(n)$  and  $D(n)$  on the complex underlying processes. An effective growth rate at low densities  $r(0)$  could be measured by monitoring the increase in fluorescent signal of a fluorescently labelled phage [56, 57] in the early stages of plaque formation. Measuring  $D(0)$  for a Fisher type expansion in phage presents some challenges, as both implicit and explicit effects would need to be accounted for. One possible approach to capture both effects would be to repeat the experiments carried out in this paper, while replacing the bacteria resistant to phage infection with one which allows phage to infect, but through a deletion to the *trxA* gene, greatly inhibits the ability of the phage to reproduce [27, 58].

An alternative approach that avoids the need for a direct measurement of the combined density-dependent diffusion consists in using the time-delayed equivalent of Eq. 11, namely:

$$\frac{\partial n}{\partial t} + \frac{\tau}{2} \frac{\partial^2 n}{\partial t^2} = \frac{\partial}{\partial x} \left( D(n) \frac{\partial n}{\partial x} \right) + nr(n) + \frac{\tau}{2} \frac{\partial}{\partial t} (nr(n)). \quad (12)$$

This represents the hyperbolic generalization of Fisher's equation, and accounts for the delay to the diffusion process caused by the incubation period  $\tau$  [59]. It has been shown that the spreading velocity  $v_F$  of the correspond-

ing linearized system is given by [60]:

$$c_F = \frac{2\sqrt{r(0)D(0)}}{1 + \frac{r(0)\tau}{2}}, \quad (13)$$

which reduces to the Fisher velocity in the case of no delay ( $\tau = 0$ ) [55]. The implicit hindrance to diffusion would then be accounted for by the terms proportional to  $\tau$  in Eq. 12 and Eq. 13, and  $D(0)$  would represent the explicit density-dependent diffusion  $D_{exp}(B_0)$  that we have measured in this work (Eq. 1). Following either of these potential approaches, and by utilising different phage, experimentally measured plaque velocities for a range of bacterial densities and life-history parameters could then be compared to the measured linear velocity of the system, and any transitions to a pushed wave investigated.

Importantly, front velocity is but one of the dynamical properties affected by a pushed transition. It has been shown, for instance, that the loss of genetic diversity during the expansion behaves qualitatively different in pulled versus pushed waves [15]. By controlling the density of host bacteria in a lawn one could tune the strength of the emergent co-operativity in an experimental expanding phage population. Either by utilising fluorescent labelled phage [56, 57], or by periodically sequencing the expansion, it should be possible to track the loss of genetic diversity over time. This would allow for the classification of expanding phage populations, without the need to map experiments to precise models of front velocity.

## VI. MATERIALS AND METHODS

### Bacterial Strains

Five strains of *E. coli* were involved in this work. The first strain, *E. coli* BW25113 (CGSC# 7636), is susceptible to phage infection. This strain was transformed previously with a plasmid expressing venus YFP to create the second strain, *E. coli* eWM43 [26]. This strain was further transformed with plasmid pAK501 (Addgene# 48107) [61], which confers resistance to chloramphenicol, to create the third strain, *E. coli* eMTH43. The fourth strain used, *E. coli*  $\Delta waaC$ , is resistant to phage infection through deletion of the *waaC* gene, the product of which is involved in the production of lipopolysaccharide, the recognition of which is essential for the adsorption of phage [27]. This strain was transformed previously with a plasmid expressing mCherry to yield the final strain *E. coli* eWM44 [26]. The strains eMTH43 and eWM44 were the two strains used respectively as the susceptible and resistant host in our experiments.

### Bacteriophage T7

The phage used in the study is the obligately lytic bacteriophage T7. The phage was originally obtained as an aliquot from the wild-type stock of the Richardson lab (Harvard Medical School, Boston, MA). To prepare stocks of this phage, phage were added to an exponentially growing liquid culture of BW25113, and incubated at 37 °C until clear. The lysate was then mixed with NaCl to a final concentration of 1.4 M. This was then spun down to remove cell debris, and the resulting supernatant was stored at 4 °C.

### Sample Preparation

To measure the diffusion coefficient of phage, 96 well plate sized omni-plates, containing 35 ml of 20 g/l agar (VWR Chemicals), with 25 g/l LB (Invitrogen) - NaCl concentration 10 g/l - and 15  $\mu\text{g/ml}$  chloramphenicol (Sigma-Aldrich) were prepared and kept at room temperature for 2 days. The presence of chloramphenicol in the plate prevents growth of the background strain eWM44, so to maintain its density constant over the course of the experiment. Plates were then refrigerated if they were to be used at a later date. Overnight liquid cultures of *E. coli* were grown from single colonies at 37 °C in 25 g/l LB with either 100  $\mu\text{g/ml}$  ampicillin (Sigma-Aldrich) or 15  $\mu\text{g/ml}$  chloramphenicol (Sigma-Aldrich) for eWM44 and eMTH43 respectively.

To create the background lawn of bacteria, the optical density at 600 nm ( $\text{OD}_{600}$ ) of the eWM44 culture was measured, and diluted with 25 g/l LB to obtain the desired density (calculated on the basis that  $\text{OD}_{600} = 0.1$  equates to  $10^8$  cells/ml). A 500  $\mu\text{l}$  droplet of this culture was then spread with glass beads (radius 4 mm) across the surface of the agar until dry. This process (a 500  $\mu\text{l}$  droplet spread with fresh beads) was repeated a further two times to achieve as uniform a distribution as possible. The plate was then left for a further 10 minutes before proceeding to the next step.

10 ml of eMTH43 overnight culture was spun down and re-suspended in fresh 25 g/l LB, so as to give an  $\text{OD}_{600}$  reading of 0.50 if diluted hundredfold. 2  $\mu\text{l}$  droplets of the concentrated culture were then pipetted onto the lawn of eWM44 in a grid like pattern, spaced approximately 1 cm apart, and left to dry (approximately 15 mins after the last droplet was pipetted). Each plate contained approximately 60 host droplets. The plate was then incubated at 37 °C for 1 hour.

10  $\mu\text{l}$  of stock T7 phage ( $10^7$  pfu/ml) was diluted in 100  $\mu\text{l}$  of black food dye. 1  $\mu\text{l}$  droplets of this dilution were pipetted onto the surface of the agar, in the gaps between the previously pipetted droplets of eMTH43, and left to dry. A schematic of the resulting set-up can be seen in Fig. 1a.

## Data Acquisition

The plates were imaged using a Zeiss Axio Zoom.V16 stereo microscope equipped with a Zeiss PlanApo Z 0.5x/0.125 FWD 114 mm objective. Images of the sample were taken every 20 minutes for a period of 24 hours. During the imaging period, the sample was kept with its lid on at 37 °C using an ibidi Multi-Well Plate Heating System.

## Data Analysis

All of the images were analysed using Fiji (v1.52h), an open source distribution of ImageJ focused on scientific image analysis [62, 63].

The time  $\Delta t$  necessary for a clearing to appear in the droplets of eMTH43, and the separation  $r$  between the point at which a clearing forms and the nearest phage droplet was recorded (Fig. 1). By measuring  $r$  and  $\Delta t$  over many droplet-droplet pairs, one can measure the mean first-passage time  $\bar{t}$  (the mean time taken for the first phage to diffuse a fixed distance  $r$ ), and calculate the rate of phage diffusion by fitting the relationship [64]:

$$r^2 = 4D\bar{t} + \text{constant}, \quad (14)$$

where  $D$  is the diffusion coefficient, and the constant arises due to the delay between the arrival of the phage and the formation of a visible plaque.

## Numerical Solutions of Reaction-Diffusion Model

We consider the scaled equations (Eq. 5) on a finite interval of length  $L_D$  with homogeneous Neumann boundary conditions. Throughout we used  $L_D = 120$  and a maximum possible time of  $\bar{t}_{max} = 50$ . Initially, we set  $\bar{B} = 1$  over the whole interval,  $\bar{V} = 1$  for  $\bar{x} \leq 2$ , and  $\bar{V} = 0$  elsewhere. There are initially no infected bacteria ( $\bar{I} = 0$ ). Solutions are determined on a mesh of uniform space and time, with divisions of  $d\bar{t} = 0.1$ , and  $d\bar{x} = 0.1$  or  $d\bar{x} = 0.2$  to give the best balance between precision and compute time for a given parameter set.

A sketch of the fronts during the expansion can be seen in Fig. 2a. The dimensionless spreading velocity  $\bar{c}$  of the front is determined by tracking the midpoint of the bacterial wave (i.e.  $\bar{B} = 0.5$ ) over time. For pulled fronts, the spreading velocity is known to demonstrate a power law convergence to an asymptotic value [65]. In the case where a steady spreading velocity was not reached, the spreading velocity was given by the asymptotic value which produced the best power law fit to the data.

The transitions between pulled, semi-pushed and fully pushed have been found to occur at specific wave velocities with respect to the linearised (Fisher) velocity  $c_F$  - the velocity determined solely by the linear dynamics at the tip of the front [15]. Pulled expansions spread with

a velocity equal to the velocity of the linearised model  $c = c_F$ , while pushed expansions spread faster [11]. The transition between semi-pushed and fully pushed occurs at a velocity of  $\frac{c}{c_F} = \frac{3}{2\sqrt{2}}$ , with waves below this velocity being semi-pushed, and above this velocity being fully pushed [15]. These thresholds have been shown to be robust to the details of the population dynamics, suggesting that they can be used as universal conditions to distinguish between the different wave classes [14].

Even though strictly speaking pulled expansions occur when the spreading velocity is equal to the velocity of the linearised model ( $c = c_F$ ), due to errors in determining the velocity over a finite time (i.e. errors due to the power law fit when determining the asymptotic velocity), we conservatively consider velocities within 1% of the linearised velocity as corresponding to pulled expansions.

A length scale characterising the width of the infected region  $\Delta\bar{x}_I$  was also computed by tracking the separation between the midpoint on the wave of uninfected bacteria ( $\bar{B} = 0.5$ ), and the midpoint on the wave of infected bacteria ( $\bar{B} + \bar{I} = 0.5$ ) over time. An average was taken over the final 20 time points for the reported value of  $\Delta\bar{x}_I$ .

## Linearised Solution of Reaction-Diffusion Model

To determine the transition between pulled, semi-pushed and fully pushed regimes, the linearised solution to the model is required. To achieve this, we first look for travelling wave solutions to Eq. 5 in the coordinate  $\bar{z} \equiv \bar{x} - \bar{c}\bar{t}$  where  $\bar{c}$  is the dimensionless front velocity.

As the components approach their limiting concentrations at the leading edge of the front, the linearised form of the model becomes valid, and so, following previous work [21, 24], we assume the concentrations take the form  $\bar{V} = a_1 \exp(-\bar{\lambda}\bar{z})$ ,  $\bar{B} = 1 - a_2 \exp(-\bar{\lambda}\bar{z})$  and  $\bar{I} = a_3 \exp(-\bar{\lambda}\bar{z})$  where  $\bar{\lambda}$  is a dimensionless width parameter, and  $a_1$ ,  $a_2$  and  $a_3$  are positive constants.

Substituting into Eq. 5 and writing in matrix notation yields:

$$\begin{pmatrix} K(\beta - 1) & -\bar{\lambda}\bar{c} & 0 \\ K(\beta - 1)(1 - e^{-\bar{\lambda}\bar{z}}) & 0 & -\bar{\lambda}\bar{c} \\ \bar{\lambda}^2 - \bar{\lambda}\bar{c} + K(\beta e^{-\bar{\lambda}\bar{z}} - 1) & 0 & 0 \end{pmatrix} \begin{pmatrix} a_1 \\ a_2 \\ a_3 \end{pmatrix} = 0. \quad (15)$$

For non-trivial solutions the determinant of the matrix is set to zero, leading to the characteristic equation:

$$\bar{\lambda}^2 - \bar{\lambda}\bar{c} + K(\beta e^{-\bar{\lambda}\bar{z}} - 1) = 0. \quad (16)$$

As we are assuming here that the front is pulled, the front propagates with the minimum possible velocity [65]:

$$\bar{c} = \min_{\bar{\lambda} > 0} [\bar{c}(\bar{\lambda})]. \quad (17)$$

By implicitly differentiating Eq. 16 with respect to  $\lambda$ , and setting  $dc/d\lambda = 0$  according to Eq. 17, this leads to the

second characteristic equation:

$$2\bar{\lambda} - \bar{c} - K\beta\bar{c}e^{-\bar{\lambda}\bar{c}} = 0. \quad (18)$$

The dimensionless spreading velocity  $\bar{c}$  is given as the unique solution to both Eq. 16 and Eq. 18.

### Analytical Model of ‘‘Implicit’’ Density Dependence

To develop a simple analytical model to describe the effect of the underlying viral dynamics on the phage diffusion, we imagine phage diffusing across a lawn of ‘‘sticky’’ penetrable disks. These disks are used to represent host bacteria cells that are able to adsorb phage for a period equivalent to the lysis time, but do not pose a hindrance to the phage through steric interactions.

In this set-up, phage diffuse through a series of discrete steps, where phage move a certain distance with each step. In any given step, the probability that a phage will become adsorbed to one of the host bacteria is  $p_\alpha\phi$ , where  $p_\alpha$  represents the probability of adsorbing when a phage encounters a host, and  $\phi$  represents the fraction of all space occupied by the host bacteria. This represents a Poisson point process, where events (adsorption) occur continuously and independently, with constant rate ( $p_\alpha\phi$ ). Therefore, the average number of steps that a phage takes before becoming adsorbed to a host is given by the expectation value of the exponential distribution,  $t_{ads} = \frac{1}{p_\alpha\phi}$ . Consequently, over the period of time  $T = t_{ads} + \tau_s$ , where  $\tau_s$  is the lysis time (in steps), the phage will only have on average actually moved for  $t_{ads}$  of that time.

This process can be thought of as a hindered diffusion process with relative diffusion coefficient equal to

$$\frac{D}{D_0} = D_{imp} = \frac{t_{ads}}{t_{ads} + \tau_s} = \frac{1}{1 + p_\alpha\tau_s\phi}, \quad (19)$$

where  $D_0$  is the free diffusion coefficient, and  $D_{imp}$  is the density-dependent diffusion coefficient resulting from the hindrance posed by the underlying viral dynamics, which we have termed the ‘‘implicit’’ density-dependence.

This can be re-written in terms of the parameters used in the main text as

$$\frac{D}{D_0} = D_{imp} = \frac{1}{1 + p_\alpha\tau_s\phi} = \frac{1}{1 + AfK_{max}}, \quad (20)$$

where  $A$  is a scaling parameter given by:

$$A = \frac{p_\alpha\tau_s\phi}{\alpha\tau B_{max}b}. \quad (21)$$

To compare the parameters used in the two descriptions, we can consider that long range diffusion will be prevented (i.e. when  $b = 1$ ) at the percolation threshold of the system  $\phi_c$ . This allows us to say that  $\phi = \phi_cb$  and  $B_{max} = \phi_c\phi_{max}$ , where  $\phi = B/\phi_{max}$ . We can then use the fact that the term  $\alpha\phi_{max}$  determines the rate at

which phage are adsorbed when in contact with bacteria (as all space is filled with bacteria at  $\phi_{max}$ ), and so, like  $p_\alpha\tau_s$ , the term  $\alpha\phi_{max}\tau$  measures the the total probability that phage will be adsorbed over a lysis time, assuming that the phage are always in contact with bacteria (i.e.  $p_\alpha\tau_s = \alpha\phi_{max}\tau$ ). This leads to a value for  $A$  of:

$$A = \frac{p_\alpha\tau_s\phi}{\alpha\tau B_{max}b} = \frac{p_\alpha\tau_s\phi_cb}{\alpha\tau\phi_c\phi_{max}b} = 1. \quad (22)$$

Consequently, the implicit density dependence can be written equivalently in terms of either parameters as:

$$\frac{D}{D_0} = D_{imp} = \frac{1}{1 + p_\alpha\tau_s\phi} = \frac{1}{1 + bK_{max}}. \quad (23)$$

### Analytical Model Predicts Multiplicative Effects of Steric Interactions and Infection Dynamic

The model introduced above can be modified to account for the presence of steric effects. In the absence of adsorption, if excluded-volume interactions were the only hindrance to diffusion, the average fraction of steps successfully jumped by phage compared to the total attempted would be  $D_{exp} = 1 - \phi$ . Although this is an approximation as it does not take into account the fact that there might be correlation between jumps, which is why it deviates from the more precise Fricke’s equation, it helps extending the analytical model in the previous section.

If we now introduce adsorption, as explained in the previous section, the average number of steps taken by phage before adsorbing to an obstacle will be  $t_{ads} = 1/p_\alpha\phi$ . In the presence of steric interactions, only a fraction  $1 - \phi$  of these steps will be successful, so that  $t_{succ} = \frac{1-\phi}{p_\alpha\phi}$ . Thus, on average, the success rate of jumping if both adsorption and steric interactions are taken into account will be:

$$\frac{D}{D_0} = D_{exp+imp} = \frac{t_{succ}}{t_{ads} + \tau_s} = \frac{1 - \phi}{1 + p_\alpha\tau_s\phi}, \quad (24)$$

which is equivalent to the product  $D_{exp}D_{imp}$ . The same argument holds if we replace the simplified  $D_{exp} = 1 - \phi$  with the more precise Fricke’s law parameterised by our experiments, generating Eq. 10.

### Implicit ‘Boost’ to Diffusion

This section will derive how the implicit diffusion rate in the UDM- can be thought of as a boost to the implicit diffusion rate in the UDM+. Here, let the proxy relative diffusion rates of the UDM+ and UDM- be denoted by  $D_{imp+}$  and  $D_{imp-}$ . Following our previous derivations, these rates are given by:

$$D_{imp\pm} = \frac{1}{1 + b_{\pm}K_{max}}, \quad (25)$$

where  $b_+ = \frac{B+I}{B_{max}}$  and  $b_- = \frac{B}{B_{max}}$ , owing to the fact that infected cells are either adsorbing or non-adsorbing in the two models.

So as to compare to the dimensionless set of parameters used in the model (where  $\bar{D} = 1$  at the expansion front), we re-scale the implicit coefficients as:

$$\bar{D}_{imp\pm} = \frac{1 + fK_{max}}{1 + \rho_{\pm} fK_{max}}, \quad (26)$$

where  $\rho_+ = \bar{B} + \bar{I}$  and  $\rho_- = \bar{B}$ .

If we then compare the ratio of the two coefficients, it can be seen that

$$\frac{\bar{D}_{imp-}}{\bar{D}_{imp+}} \approx \frac{1 + fK_{max}}{1 + \bar{B}fK_{max}} \frac{1 + (\bar{B} + \bar{I})fK_{max}}{1 + fK_{max}}, \quad (27)$$

$$\approx \frac{1 + (\bar{B} + \bar{I})fK_{max}}{1 + \bar{B}fK_{max}}, \quad (28)$$

$$\approx 1 + \frac{\bar{I}fK_{max}}{1 + \bar{B}fK_{max}}. \quad (29)$$

It should be noted that the approximation arises from the assumption that the bacterial curves  $\bar{B}$  and  $\bar{I}$  are the same in both expansions. Therefore we can see that we can write  $\bar{D}_{imp-}$  in terms of  $\bar{D}_{imp+}$  as

$$\bar{D}_{imp-} \approx (1 + \psi)\bar{D}_{imp+}; \quad \psi = \frac{\bar{I}fK_{max}}{1 + \bar{B}fK_{max}}. \quad (30)$$

### Diffusion Profiles

Fig. 4b shows the proxy diffusion rates of each of the model variants as a function of position across the expansion front. To generate this, the population profiles  $\bar{V}$ ,  $\bar{B}$  and  $\bar{I}$  of each of the model variants were taken at the maximum time at which they were determined (so as to be as close to the steady state as possible), and then shifted in space so that the position of the half max point on the uninfected bacterial curves ( $\bar{B} = 0.5$ ) aligned in each of the model variants. These population curves were then used to determine the proxy dimensionless diffusion coefficients.

### ACKNOWLEDGMENTS

We acknowledge help from R. Majed in performing bacterial transformations. MH acknowledges studentship funding from EPSRC under grant number EP/R513180/1. TL acknowledges college grant from St Edmund Hall. This work was performed using resources provided by the Cambridge Service for Data Driven Discovery (CSD3) operated by the University of Cambridge Research Computing Service, provided by Dell EMC and Intel using Tier-2 funding from the Engineering and Physical Sciences Research Council (capital grant EP/P020259/1), and DiRAC funding from the Science and Technology Facilities Council.

### Appendix A: Monte Carlo Simulations of Diffusion

Monte Carlo simulations of point-like phage diffusing across a lawn of penetrable “sticky” disks, representing adsorbing host bacteria in the absence of steric effects, show that the hindrance posed by the underlying viral is equivalent to an “implicit” density-dependent reduction in diffusion  $D_{imp}$  (Fig. 7). This is in agreement with the analytical model discussed in the main text (Eq. 6 and Methods). Additionally, the Monte Carlo simulations show that the implicit density-dependent diffusion  $D_{imp}$  does not depend on the adsorption rate and lysis time independently, but only depends on their product (Fig. 7). This confirms the prediction of the analytical model of implicit density-dependence (see Methods), and the dependence only on  $K = \alpha\tau B_0$  that emerges in the UDMs.

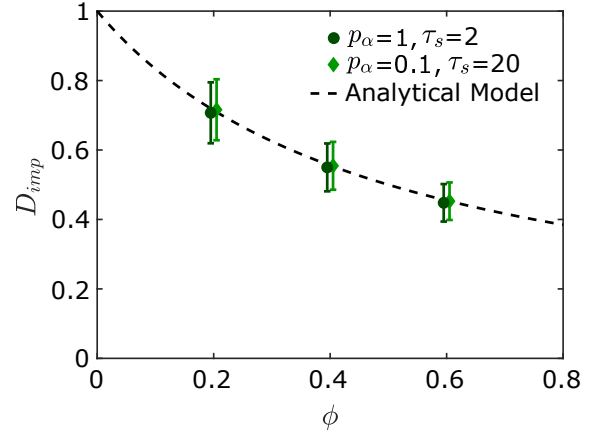


FIG. 7. Monte Carlo simulations of point-like phage diffusing through a field of penetrable “sticky” obstacles results in an “implicit” density-dependent diffusion rate  $D_{imp}$ , and confirms that this does not depend on the probability of binding  $p_\alpha$  and the lysis time  $\tau_s$  independently, but rather depends only on their product. Simulation data offset slightly for clarity. Analytical model provided by Eq. 23 (see Methods).

The simulations are carried out in a 2D box with period boundary conditions, populated with circular obstacles of fixed diameter  $d_{obs}$ , representing a lawn of host bacteria cells. Obstacles are generated with random center co-ordinates within the boundary of the lawn until a fraction  $\phi$  of the area of the lawn is occupied (obstacles may overlap). We use *sticky penetrable* obstacles to mimic the implicit hindrance to diffusion due to infection dynamics. A number of point-like tracers (representing phage) are placed on the lawn and start to diffuse in discrete steps. At each step, every free tracer proposes a new random co-ordinate within a circular region of radius  $r_{step}$  of its current position. If there is no obstacle at the new co-ordinate, the tracer jumps to the new position. If, however, there is an obstacle at the new co-ordinate, the tracer jumps to the new position, and then has a proba-

bility  $p_\alpha$  of adsorbing to that obstacle. Upon successful adsorption, the tracer remains bound to the obstacle for a number of steps  $\tau_s$  (representing the viral incubation period).

The size of the lawn is  $1000 d_{obs}$ , and  $r_{step} = 5 d_{obs}$ . We use 100 phages for each simulation, and run 100 simulations. The simulations are run for 3 million steps, to observe equilibration of the diffusive behavior.

### Appendix B: The Impact of Burst Size

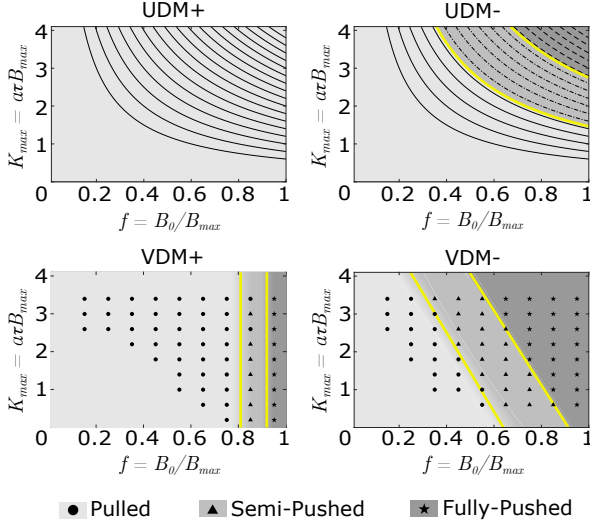


FIG. 8. Phase diagrams showing the expansion types for the four model variants as a function of  $f$  and  $K_{max}$  -  $\beta=20$  throughout. As can be seen by comparison to Fig. 3, the qualitative behaviour of the transitions in each of the models remains the same, and can be characterised using the same parameters  $K_{s,p}$ ,  $m_{s,p}$ ,  $a_{s,p}$  and  $f_{s,p}$ . As before, lines in the UDMs, and data points in the VDMs indicate the parameter combinations for which numerical integration was performed, and velocities calculated. Transition boundaries (yellow lines) are inferred from the data points calculated.

In Fig. 8 we present the equivalent phase diagrams as shown in Fig. 3 for a different burst size  $\beta=20$ . It can be seen by comparing both Figures that the qualitative behaviour of the transitions remains unchanged: in the UDM-, transitions are characterised by constant values of  $K_s$  and  $K_p$ ; in the VDM-, transitions are approximately straight lines characterised by gradients  $m_s$  and  $m_p$ , and intercepts  $a_s$  and  $a_p$ ; in the VDM+, transitions are largely independent of  $K_{max}$ , and occur at critical values  $f_s$  and  $f_p$ .

As it seems the behaviour can be characterised in the same manner when burst size is changed, we simplify our examination by focusing only on how the burst size alters these specific characteristic parameters. Rather than attempting to produce the whole phase diagram for each of the models at various  $\beta$ , as this is very computationally intensive when  $\beta$  is either small or large, we instead

choose a specific  $K_{max}$  value, and for various values of  $\beta$ , we vary  $f$  at this  $K_{max}$  value. From this, the parameters  $K_{s,p}$  and  $f_{s,p}$  as a function of  $\beta$  can be easily obtained.

To investigate the behaviour in the VDM- from only one pair of transition points, we assume that  $m_{s,p}$  are constant with burst size, and calculate how  $a_{s,p}$  vary as a result. In the two cases where the full phase diagrams were computed, the transition gradients were calculated as  $m_s = -0.125(5)$ ,  $-0.091(11)$  and  $m_p = -0.097(5)$ ,  $-0.101(2)$  for  $\beta = 50, 20$ , indicating agreement to within  $2\sigma$  and  $1\sigma$  respectively.

We find that while the general shape of the transitions for the model variants does not depend on  $\beta$  (Fig. 8), the exact location of the transitions are affected (Fig. 9). The dependence of all of the transition parameters on  $\beta$  is similar across models. Above  $\beta \approx 40$ , the parameters exhibit only a weak dependence on burst size, whereas when  $\beta$  decreases below this value, the transition parameters also decrease, increasing the parameter range of  $K_{max}$  and  $f$  in which we observe a pushed wave.

This behaviour qualitatively matches the dependence of the spreading velocity of the linearised model  $\bar{c}_F$  on burst size (Fig. 10). While  $f$  and  $K_{max}$  determine the ability of phage in the bulk to catch up to the front and contribute to the dynamics, either due to explicit or implicit hindrance to diffusion,  $\beta$  only contributes to the phage growth rate and, as a result, the velocity of the front. At lower values of  $\beta$ , the spreading velocity is greatly reduced as the limited number of phage released at the tip after each lysis event struggle to clear the host cells around them, allowing the phage in the back to catch up more easily, regardless of the mechanism, and contribute to the expansion. As burst size is increased however, the opposite is true, although the velocity gains that come with increased  $\beta$  become increasingly marginal, as the uninfected host within the vicinity of recently lysed cells become saturated with newly released phage.

### Appendix C: Ratio of Explicit to Implicit Effects

Here we present a plot of the ratio of the explicit boost to diffusion  $\bar{D}_{exp}$  to the implicit boost to diffusion  $(1+\psi)$ , as a function of  $f$  and  $K_{max}$ . It can be seen in Fig. 11 that the implicit boost is dominant at large  $K_{max}$ , while the explicit boost dominates at low  $K_{max}$ .

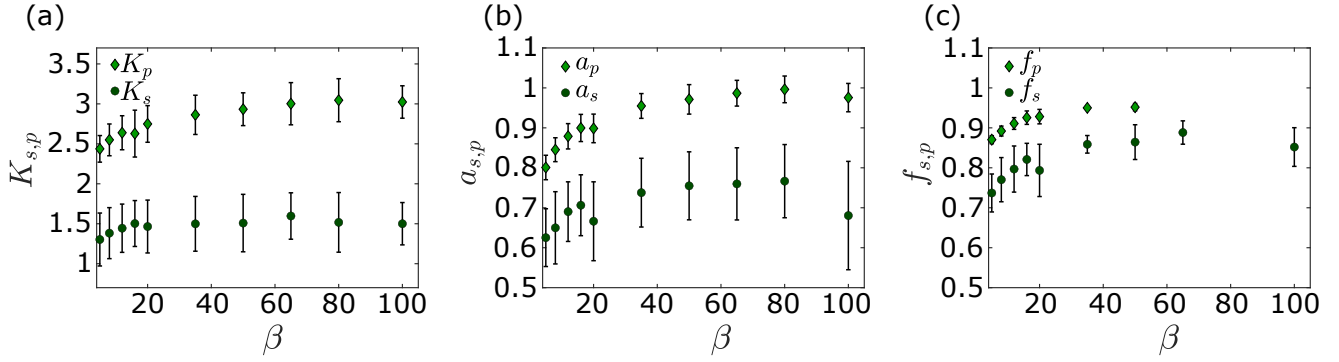


FIG. 9. Behavior of the critical parameters describing the location of the transitions (Fig. 3 and Fig. 8) as a function of burst size  $\beta$ . (a): Critical values  $K_s$  and  $K_p$  in the UDM-. (b): Critical values  $a_s$  and  $a_p$  in the VDM-, calculated from transition locations at  $K_{max}=2.2$ , assuming the gradients of the transitions  $m_s$  and  $m_p$  are approximately constant when varying  $\beta$ , to maintain computational feasibility. (c): Critical values  $f_s$  and  $f_p$  in the VDM+, similarly calculated from transition locations at  $K_{max}=2.2$ . Fully pushed transitions were not observed at high  $\beta$  due to impractical compute times when  $f > 0.95$ . In each case, we assume a 1% error in the model velocities as before, and by shifting the velocities accordingly, we determine the resultant shift in the transition parameters (error bars shown).

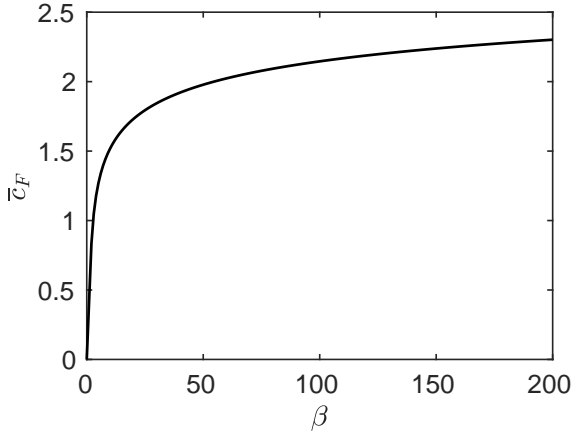


FIG. 10. Spreading velocity of the linearised model for  $K = 1.0$  as a function of burst size  $\beta$  (in the linearised model,  $K$  and  $\beta$  are the only independent parameters).

---

[1] R. I. Colautti and S. C. H. Barrett, Rapid adaptation to climate facilitates range expansion of an invasive plant., *Science* (New York, N.Y.) **342**, 364 (2013).  
 [2] L. L. Cavalli-Sforza, P. Menozzi, and A. Piazza, Demic expansions and human evolution, *Science* **259**, 639 (1993).  
 [3] N. A. Rosenberg, J. K. Pritchard, J. L. Weber, H. M. Cann, K. K. Kidd, L. A. Zhivotovsky, and M. W. Feldman, Genetic Structure of Human Populations, *Science* **298**, 2381 LP (2002).  
 [4] S. Ramachandran, O. Deshpande, C. C. Roseman, N. A. Rosenberg, M. W. Feldman, and L. L. Cavalli-Sforza, Support from the relationship of

genetic and geographic distance in human populations for a serial founder effect originating in Africa., *Proceedings of the National Academy of Sciences of the United States of America* **99**, 2268 (2002).  
 [5] A. R. Templeton, Out of Africa again and again, *Nature* **416**, 45 (2002).  
 [6] I.-C. Chen, J. K. Hill, R. Ohlemüller, D. B. Roy, and C. D. Thomas, Rapid range shifts of species associated with high levels of climate warming., *Science* (New York, N.Y.) **333**, 1024 (2011).  
 [7] G. M. Hewitt, Some genetic consequences of ice ages, and their role in divergence and speciation, *Biological Journal of the Linnean Society* **58**, 247 (1996).

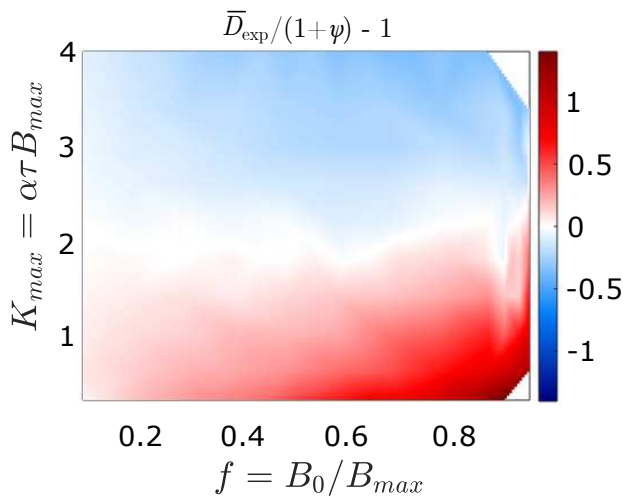


FIG. 11. The ratio of the explicit boost to diffusion  $\bar{D}_{exp}$  to the implicit boost to diffusion  $(1 + \psi)$ , as a function of  $f$  and  $K_{max}$ .

- [8] G. Hewitt, The genetic legacy of the quaternary ice ages, *Nature* **405**, 907 (2000).
- [9] O. Hallatschek and D. R. Nelson, Gene surfing in expanding populations, *Theoretical Population Biology* **73**, 158 (2008).
- [10] S. Klopstein, M. Currat, and L. Excoffier, The Fate of Mutations Surfing on the Wave of a Range Expansion, *Molecular Biology and Evolution* **23**, 482 (2006).
- [11] W. van Saarloos, Front propagation into unstable states, *Physics Reports* **386**, 29 (2003).
- [12] L. Roques, J. Garnier, F. Hamel, and E. K. Klein, Allee effect promotes diversity in traveling waves of colonization., *Proceedings of the National Academy of Sciences of the United States of America* **109**, 8828 (2012).
- [13] W. C. Allee, Co-Operation Among Animals, *American Journal of Sociology* **37**, 386 (1931).
- [14] G. Birzu, S. Matin, O. Hallatschek, and K. S. Korolev, Genetic drift in range expansions is very sensitive to density dependence in dispersal and growth, *Ecology Letters* **22**, 1817 (2019).
- [15] G. Birzu, O. Hallatschek, and K. S. Korolev, Fluctuations uncover a distinct class of traveling waves, *Proceedings of the National Academy of Sciences of the United States of America* **115**, E3645 (2018).
- [16] D. M. Johnson, A. M. Liebhold, P. C. Tobin, and O. N. Bjørnstad, Allee effects and pulsed invasion by the gypsy moth, *Nature* **444**, 361 (2006).
- [17] R. R. Veit and M. A. Lewis, Dispersal, population growth, and the allee effect: Dynamics of the house finch invasion of eastern North America, *American Naturalist* **148**, 255 (1996).
- [18] S. R. Gandhi, E. A. Yurtsev, K. S. Korolev, and J. Gore, Range expansions transition from pulled to pushed waves as growth becomes more cooperative in an experimental microbial population, *Proceedings of the National Academy of Sciences* **113**, 6922 (2016).
- [19] S. R. Gandhi, K. S. Korolev, and J. Gore, Cooperation mitigates diversity loss in a spatially expanding microbial population, *Proceedings of the National Academy of Sciences of the United States of America* **116**, 23582 (2019).
- [20] E. Matthysen, Density-dependent dispersal in birds and mammals, *Ecography* **28**, 403 (2005).
- [21] J. Yin and J. S. McCaskill, Replication of Viruses in a Growing Plaque - A Reaction-Diffusion Model, *Biophysical Journal* **61**, 1540 (1992).
- [22] L. J. Alvarez, P. Thomen, T. Makushok, and D. Chatenay, Propagation of fluorescent viruses in growing plaques, *Biotechnology and Bioengineering* **96**, 615 (2007).
- [23] L. You and J. Yin, Amplification and Spread of Viruses in a Growing Plaque, *Journal of Theoretical Biology* **200**, 365 (1999).
- [24] J. Fort and V. Méndez, Time-delayed spread of viruses in growing plaques, *Physical Review Letters* **89**, 10.1103/PhysRevLett.89.178101 (2002).
- [25] V. Ortega-Cejas, J. Fort, V. Méndez, and D. Campos, Approximate solution to the speed of spreading viruses, *Physical Review E* **69**, 031909 (2004).
- [26] W. Möbius, A. W. Murray, and D. R. Nelson, How Obstacles Perturb Population Fronts and Alter Their Genetic Structure, *PLOS Computational Biology* **11**, e1004615 (2015).
- [27] U. Qimron, B. Marintcheva, S. Tabor, and C. C. Richardson, Genomewide screens for *Escherichia coli* genes affecting growth of T7 bacteriophage, *Proceedings of the National Academy of Sciences* **103**, 19039 LP (2006).
- [28] H. Fricke, A mathematical treatment of the electric conductivity and capacity of disperse systems I. The electric conductivity of a suspension of homogeneous spheroids, *Physical Review* **24**, 575 (1924).
- [29] J. Crank and E. P. J. Crank, *The Mathematics of Diffusion*, Oxford science publications (Clarendon Press, 1979).
- [30] D. Stollar and L. Levine, Two-dimensional immunodiffusion, *Methods in Enzymology* **6**, 848 (1963).
- [31] H. W. Ackermann, Classification of tailed enterobacteria phages, *Pathologie-biologie* **24**, 359 (1976).
- [32] D. A. Jones, H. L. Smith, H. R. Thieme, and G. Röst, Coexistence of *Escherichia coli* and bacteriophage T7 in a petri dish, *SIAM Journal on Applied Mathematics* **72**, 670 (2012).
- [33] D. R. Amor and J. Fort, Virus infection speeds: Theory versus experiment, *Physical Review E* **82**, 061905 (2010).
- [34] D. R. Amor and J. Fort, Cohabitation reaction-diffusion model for virus focal infections, *Physica A: Statistical Mechanics and its Applications* **416**, 611 (2014).
- [35] V. de Rioja, J. Fort, and N. Isern, Front propagation of *Escherichia coli* virus mutants, *Journal of Theoretical Biology* **385**, 112 (2015).
- [36] H. J. Park and C. S. Gokhale, Ecological feedback on diffusion dynamics, *Royal Society Open Science* **6**, 181273 (2019).
- [37] M. E. Cates, D. Marenduzzo, I. Pagonabarraga, and J. Tailleur, Arrested phase separation in reproducing bacteria creates a generic route to pattern formation, *Proceedings of the National Academy of Sciences of the United States of America* **115**, E3645 (2018).
- [38] D. Panja, Effects of fluctuations on propagating fronts, *Physics Reports* **393**, 87 (2004).
- [39] S. Peischl, M. Kirkpatrick, and L. Excoffier, Expansion speed and the evolutionary dynamics of a species range., *The American naturalist* **185**, 81 (2015).
- [40] L. Bosshard, I. Dupanloup, O. Tenaillon, R. Bruggmann, M. Ackermann, S. Peischl, and L. Excoffier, Accumulation of mutations in a growing Bacterial Range



- Expansions, *Genetics* **207**, 669 (2017).
- [41] T. Matsuyama, K. Komatsu, A. Nakahara, and M. Matsushita, Experimental Investigation on the Validity of Population Dynamics Approach to Bacterial Colony Formation, *Journal of the Physical Society of Japan* **63**, 1205 (1994).
- [42] A. Giometto, A. Rinaldo, F. Carrara, and F. Altermatt, Emerging predictable features of replicated biological invasion fronts, *Proceedings of the National Academy of Sciences of the United States of America* **111**, 2974 (2014).
- [43] S. J. Labrie, J. E. Samson, and S. Moineau, Bacteriophage resistance mechanisms, *Nature Reviews Microbiology* **8**, 317 (2010).
- [44] V. Braun, H. Killmann, and C. Herrmann, Inactivation of FhuA at the cell surface of *Escherichia coli* K-12 by a phage T5 lipoprotein at the periplasmic face of the outer membrane, *Journal of Bacteriology* **176**, 4710 (1994).
- [45] I. Pedruzzi, J. P. Rosenbusch, and K. P. Locher, Inactivation in vitro of the *Escherichia coli* outer membrane protein FhuA by a phage T5-encoded lipoprotein, *FEMS Microbiology Letters* **168**, 119 (1998).
- [46] L. L. Perry, P. SanMiguel, U. Minocha, A. I. Terekhov, M. L. Shroyer, L. A. Farris, N. Bright, B. L. Reuhs, and B. M. Applegate, Sequence analysis of *Escherichia coli* O157:H7 bacteriophage  $\Phi$ v10 and identification of a phage-encoded immunity protein that modifies the O157 antigen, *FEMS Microbiology Letters* **292**, 182 (2009).
- [47] G. J. Newton, C. Daniels, L. L. Burrows, A. M. Kropinski, A. J. Clarke, and J. S. Lam, Three-component-mediated serotype conversion in *Pseudomonas aeruginosa* by bacteriophage D3, *Molecular Microbiology* **39**, 1237 (2004).
- [48] J. Bondy-Denomy, J. Qian, E. R. Westra, A. Buckling, D. S. Guttman, A. R. Davidson, and K. L. Maxwell, Prophages mediate defense against phage infection through diverse mechanisms, *ISME Journal* **10**, 2854 (2016).
- [49] S. van Houte, A. Buckling, and E. R. Westra, Evolutionary Ecology of Prokaryotic Immune Mechanisms., *Microbiology and molecular biology reviews : MMBR* **80**, 745 (2016).
- [50] D. Walsh and M. H. Naghavi, Exploitation of Cytoskeletal Networks during Early Viral Infection, *Trends in Microbiology* **27**, 39 (2019).
- [51] V. Doceul, M. Hollinshead, L. Van Der Linden, and G. L. Smith, Repulsion of superinfecting virions: A mechanism for rapid virus spread, *Science* **327**, 873 (2010).
- [52] J. Yin, Evolution of bacteriophage T7 in a growing plaque., *Journal of Bacteriology* **175**, 1272 LP (1993).
- [53] M. Choua and J. A. Bonachela, Ecological and evolutionary consequences of viral plasticity, *American Naturalist* **193**, 346 (2019).
- [54] L. Vidakovic, P. K. Singh, R. Hartmann, C. D. Nadell, and K. Drescher, Dynamic biofilm architecture confers individual and collective mechanisms of viral protection, *Nature Microbiology* **3**, 26 (2018).
- [55] R. A. Fisher, The Wave of Advance of Advantageous Genes, *Annals of Eugenics* **7**, 355 (1937).
- [56] E. J. Sloatweg, H. J. H. G. Keller, M. A. Hink, J. W. Borst, J. Bakker, and A. Schots, Fluorescently labeled bacteriophage lambda: translational frameshift, *Nucleic Acids Research* **34**, e137 (2006).
- [57] S. Huang, H. Wang, C. A. Carroll, S. J. Hayes, S. T. Weintraub, and P. Serwer, Analysis of proteins stained by Alexa dyes, *Electrophoresis* **25**, 779 (2004).
- [58] T. Baba, T. Ara, M. Hasegawa, Y. Takai, Y. Okumura, M. Baba, K. A. Datsenko, M. Tomita, B. L. Wanner, and H. Mori, Construction of *Escherichia coli* K-12 in-frame, single-gene knockout mutants: The Keio collection, *Molecular Systems Biology* **2**, 10.1038/msb4100050 (2006).
- [59] V. Méndez and J. Camacho, Dynamics and thermodynamics of delayed population growth, *Physical Review E - Statistical Physics, Plasmas, Fluids, and Related Topics* **79**, 046111 (2009).
- [60] J. Fort and V. Méndez, Time-delayed theory of the neolithic transition in europe, *Physical Review Letters* **82**, 867 (1999).
- [61] A. Kaczmarczyk, J. A. Vorholt, and A. Francez-Charlot, Cumate-inducible gene expression system for sphingomonads and other Alphaproteobacteria, *Applied and Environmental Microbiology* **79**, 6795 (2013).
- [62] J. Schindelin, I. Arganda-Carreras, E. Frise, V. Kaynig, M. Longair, T. Pietzsch, S. Preibisch, C. Rueden, S. Saalfeld, B. Schmid, J.-Y. Tinevez, D. J. White, V. Hartenstein, K. Eliceiri, P. Tomancak, and A. Cardona, Fiji: an open-source platform for biological-image analysis, *Nature Methods* **9**, 676 (2012).
- [63] C. T. Rueden, J. Schindelin, M. C. Hiner, B. E. DeZonia, A. E. Walter, E. T. Arena, and K. W. Eliceiri, ImageJ2: ImageJ for the next generation of scientific image data, *BMC Bioinformatics* **18**, 529 (2017).
- [64] G. Klein, Mean first-passage times of Brownian motion and related problems, *Proceedings of the Royal Society of London. Series A. Mathematical and Physical Sciences* **457**, 1037 (1999).
- [65] U. Ebert and W. Van Saarloos, Front propagation into unstable states: Universal algebraic convergence towards uniformly translating pulled fronts, *Physica D: Nonlinear Phenomena* **146**, 1 (2000).